Journal of the Serbian Chemical Society
JSCS-info@shd.org.rs • www.shd.org.rs/JSCS
J. Serb. Chem. Soc. *89* (2) 231–244 (2024)
JSCS–5717
Original scientific paper
Published 2 March 2024

Removal of lead and cadmium from aqueous solution using octacalcium phosphate as an adsorbent

MILJANA M. MIRKOVIĆ[1]*, IVAN D. BRACANOVIĆ[1#], ALEKSANDAR D. KRSTIĆ[2#], DUNJA D. ĐUKIĆ[3], VLADIMIR M. DODEVSKI[1] and ANA M. KALIJADIS[1]

[1]*Department of Materials, Vinča Institute of Nuclear Sciences – National Institute of the Republic of Serbia, University of Belgrade, Mike Petrovića Alasa 12–14, 11000 Belgrade, Serbia,* [2]*Department of Physical Chemistry, Vinča Institute of Nuclear Sciences – National Institute of the Republic of Serbia, University of Belgrade, Mike Petrovića Alasa 12–14, 11000 Belgrade, Serbia and* [3]*University of Belgrade, Faculty of Biology, Studentski Trg 16, 11000 Belgrade, Serbia*

(Received 15 September, revised 4 October, accepted 26 December 2023)

Abstract: Octacalcium phosphate (OCP) is a material from the calcium phosphate group with a crystal structure similar to hydroxyapatite. The removal process of lead and cadmium in aqueous solution using octacalcium phosphate material was investigated. OCP material was synthesized by the solution precipitation method. The structural and phase properties of OCP before and after the removal process were determined by the X-ray diffraction (XRD) method. Microstructural and semi-quantitative analysis of the material was investigated by scanning electron microscopy and energy dispersive X-ray spectroscopy (SEM-EDS). Characteristic bands and functional group determination were revealed using the Fourier-transform infrared spectroscopy with attenuated total reflection (FTIR-ATR). As target pollutants, Cd(II) and Pb(II) were chosen in adsorption experiments. Results show that OCP in the first 10 min has a very fast removal rate for Pb(II); the equilibrium state was reached after 10 min with more than 98 % adsorption efficiency. Results for Cd(II), results showed the same removal rate but somewhat lower adsorption efficiency, amounted to approximately 63 %.

Keywords: calcium phosphate material; adsorption; water purification; heavy metals.

INTRODUCTION

Due to their exceptional crystallographic, ecologically acceptable, non-toxic, and biocompatible properties, materials from the calcium phosphate group have a

* Corresponding author. E-mail: miljanam@vin.bg.ac.rs
# Serbian Chemical Society member.
https://doi.org/10.2298/JSC230915104M

significantly wide range of uses. One of the interesting ones from this group is octacalcium phosphate (OCP), with particularly unique properties,[1] next to hydroxyapatite (HA), which presents the most common calcium phosphate materials with a wide range of uses.[2,3] Octacalcium phosphate stimulates bone regeneration due to the chemical characteristics of this material, in which Ca^{2+} or PO_4^{3-} are released from the structure, and bone growth occurs in a certain direction; this activity helps the process of bone regeneration and conversion of OCP to HA.[4] Taking into account that certain good structural and, therefore, chemical properties of octacalcium phosphate can be designed by various synthesis methods, this material also can be used as an adsorbent for the removal of organic pollutants from aqueous solutions or a cation exchanger for water defluoridation.[5,6]

The possibility of using octacalcium phosphate material as a potential remover for the immobilization of organic molecules but also heavy metals, regarding its non-stoichiometric composition and structural defects at calcium ion sites and phosphate ion lattice positions, which can be replaced with cationic and anionic ions in structure.[2,7] This material has an interesting layered structure, where the HPO_4^{2-} in a hydrated layer of OCP can be replaced and stacked in an apatite layer.[1,8] In the previous studies, it's been reported that interlayers in OCP structure recognize the chirality of some organic compounds during the incorporation process.[8] Various syntheses of this material exist and have been used so far. However, precipitation is one of the simplest and most commonly used methods for obtaining materials with precisely defined characteristics.[10–13]

The main idea of this work is the synthesis of pure octacalcium phosphate material using acetate solutions as a source of calcium and hydrogen phosphate as a source of phosphorus group for its synthesis relying on ecological and cheaper synthesis methods using precursors other than nitrates or phosphoric acid. The study's main goal was to define the morphological and crystallographic parameters of the material obtained, which was used to remove heavy metal ions such as Cd(II) and Pb(II). The results of this study show the benefit of using octacalcium phosphate, which is non-toxic to the environment, where its disposal in the ecosystem represents a biofertilizer because it becomes a source of phosphorus and calcium for plants.[13]

EXPERIMENTAL

Octacalcium phosphate powder (OCP) was synthesized by a slightly modified solution-precipitation method, than the previously published,[11] by titration of 250 mL $Ca(CH_3COO)_2$ (Sigma Aldrich, *p.a.*) solution with a molar concentration of 0.04 M with 750 mL $NaH_2PO_4{\cdot}H_2O$ (Kemika, Zagreb, *p.a.*) solution with molar concentration 0.013 M. The temperature during titration synthesis was adjusted to 60 °C, and the pH value of approximately 5 pH units was maintained throughout the titration process, checked by pH meter (LLG Labware, Meckenheim, Germany). The solution in the beaker was stirred at 100 rpm, and the solution in the burette was set to drip one drop per second. After synthesis, the precipitate was transferred to a fine-grade filter paper and washed three times in distilled water and once in

alcohol, after which it was dried at 40 °C for 12 h. As a final result, fine white powder was obtained.

Structural and phase characteristics of the synthesized material were examined by the X-ray diffraction method (XRD) on a polycrystalline sample using a Siemens D500 X-ray diffractometer with CuKα radiation and Ni filter, in the 2θ range from 10 to 60°, with a scanning step size of 0.02, and scanning time of 0.5 s per step. Find It Inorganic Crystal Structure Database was used for structural data calculation and phase identification of octacalcium phosphate, using card number: ICSD #65347, and PDF2 Release 2023, using card numbers: 01-071-5049 for hydroxyapatite and 01-087-2477 for decalead hexakis(phosphate(V)) dihydroxide. Crystallite sample sizes were calculated using the Scherrer equation,[15] and structural parameters were obtained by the Powder Cell crystallographic program.[16]

The sample's morphology and surface properties were investigated using a JEOL JSM--6610LV scanning electron microscope. Before semi-quantitative EDS analysis, the unpolished sample was coated with Au – thickness 18.0 nm.

Fourier transform infrared spectroscopy with attenuated total reflection (FTIR-ATR) was used to analyze surface functional groups and the chemical nature of the OCP sample. FTIR--ATR spectra were recorded on a Thermo Fisher Scientific spectrometer, model Nicolet IS 5. For spectra processing, the Omnic program (Thermo Fisher Scientific) was used.

For adsorption kinetics experiments, Cd(II) and Pb(II) were chosen as target pollutants. The adsorbate solution was prepared from the mixture of nitrate salts, $Cd(NO_3)_2$ and $Pb(NO_3)_2$. The 20 mg of OCP sample was measured and added to the plastic tube containing 50 cm^3 of Cd(II) and Pb(II) mixture solution concentration of 40 mg/dm^3 of each pollutant. Then, the prepared mixture was shaken at 180 rpm for 24 h, and 1 cm^3 of aliquot was taken at intervals, 10, 20, 30, 60, 120, 180, 300 min and 24 h. The pH value of 40 ppm adsorbate solution was 5.5, and that value was chosen for experiments. The reason for that lies in the fact that higher pH values (pH > 6) lead to the formation of insoluble metal hydroxides, while lower pH values (pH < 4) lead to the competitive adsorption between positive Cd(II), Pb(II) ions and protons. After adsorption, the aliquot was properly diluted, acidified with HNO_3, passed through a 0.45 μm PTFE filter, and analyzed by ICP-OES spectrometer (ThermoFisher Scientific ICAP duo 7400). All adsorption experiments were performed at 25 °C in duplicate. The blank probe was also prepared. The removal efficiency of OCP for each contaminant at time τ was calculated by the following equation:[17]

$$\text{Removal} = 100\frac{C_0 + C_t}{C_0} \tag{1}$$

where C_0 and C_t (mg/dm^3) are the initial and concentration at time t (min) of pollutants, respectively.

For analysis of the adsorption kinetics study, pseudo-first-order and pseudo-second-order were used as theoretical models. The equation of pseudo-first-order is given as:[17]

$$Q_t = Q_e(1 - e^{-k_1 t}) \tag{2}$$

Where Q_t (mg/g) is the amount of adsorbed pollutant at time t (min), Q_e (mg/g) is the initial pollutant concentration in equilibrium, and k_1 (1/min) is the pseudo-first-order rate constant.

The equation of pseudo-second-order is given as:[17]

$$Q_t = Q_e\left(\frac{1}{Q_e} + k_2 + t\right)^{-1} \quad (3)$$

where k_2 (g/mg min) was the pseudo-second-order rate constant.

The parameters k_1, k_2 and Q_e were obtained from the intercept and slope of the Q_t *versus* t.

The adsorption isotherms were investigated to clarify the interaction between pollutants and OCP in solution at equilibrium and determine maximum adsorption capacity.[18] The mixture was prepared by the same procedure that was mentioned above in the concentration range 40–500 mg/dm^3 per pollutant. The prepared mixture was shaken at 200 rpm, the pH value of the adsorbate solution was 5.5, and the equilibration time was 3 h. After equilibration, 1 cm^3 of mixture was taken, properly diluted, and analyzed by ICP-OES. All adsorption experiments were performed at 25 °C in duplicate. The blank probe was also prepared. The following equation calculated the adsorption capacity:[17]

$$Q_e = \frac{V(C_0 - C_e)}{W} \quad (4)$$

where Q_e is the adsorbed amount of pollutant (mg/g), W is the mass of OCP (g), V is the volume of sample aliquot (cm^3), and C_0 and C_e are the initial and equilibrium concentrations of adsorbed pollutant.

Langmuir and Freundlich's isotherms were used as theoretical models to analyze adsorption isotherms. The general Langmuir equation was presented as follows:[17]

$$Q_e = \frac{Q_{max} b C_e}{1 + b C_e} \quad (5)$$

where Q_{max} is the theoretical maximum adsorption capacity of the adsorbent (mg of pollutant per gram of adsorbent, mg/g), b is the constant related to the heat of adsorption (dm^3/g).

The Freundlich isotherm can be represented as follows:[17]

$$Q_e = K_f C_e^{1/n_F} \quad (6)$$

Where K_f is the Freundlich empirical constant related to the adsorption capacity, (mg/g) (dm^3/mg))$^{1/n}$; $1/n_F$ is the heterogeneity factor.

RESULTS AND DISCUSSION

SEM micrographs with EDS analysis of obtained OCP material are presented in Fig. 1. Fig. 1a represents agglomerates with sizes in diameters of approximately 35 μm. The morphology of agglomerates is in spherical forms. Fig. 1b shows the detailed morphology of synthesized OCP powder. Proper crystal grains of OCP have plate-like morphology, which agrees with the precipitation method of synthesis.[19] Also, this kind of crystal formation is known in the literature as a petal-like structure.[20] Prismatic plate-like grains are stacked together in such a way that they form the appearance of a blooming flower.

Based on obtained and calculated EDS spectra, the Ca/P ratio is 1.33, typical for octacalcium phosphate materials.[21]

Fig. 2a shows the XRD pattern corresponding to synthesized OCP material. Based on the presented results, slightly wider peaks with a slightly higher baseline indicate a small crystallite size in the material, obtained by the precipitation

method of synthesis.[11–13,15,16,22] Based on the results presented, the material reveals sharp and well-defined peaks indicating proper structural arrangement. Peaks in the 2θ region from about 35 to 55° have higher intensities, which we can assume is a preferential orientation created during the sample preparation. This occurs when plate-like crystals are stacking during the application of the sample to the carrier. This phenomenon often leads to the increment of peak intensities of specific monolayer reflections.[23]

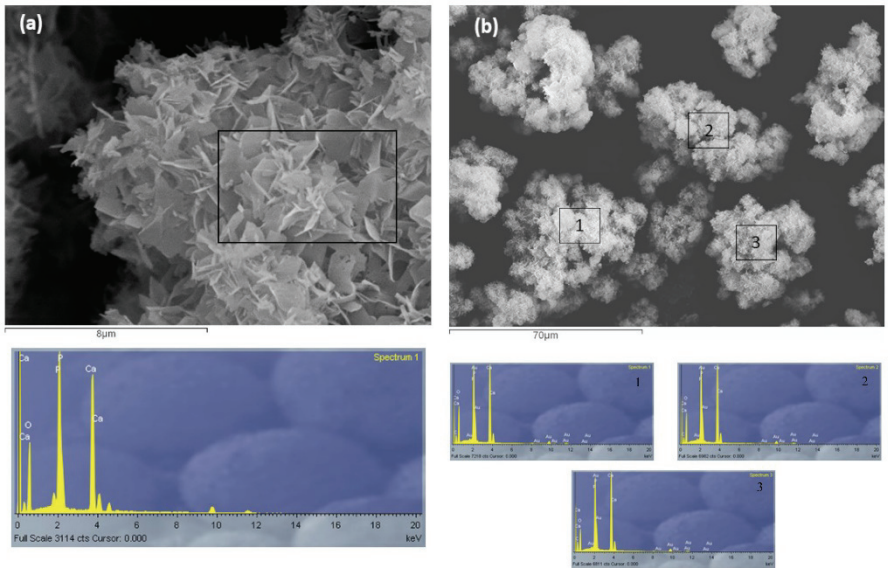

Fig. 1. Micrographs of OCP: a) Lower magnification presentation with EDS spectra, b) enlarged detail with EDS spectrum.

Refinement of structural parameters of the OCP sample is done using the Powder Cell program and ICSD file number 65347, space group $P\,\overline{1}$. The results of refinement are presented in Table I.

Structural results for OCP shown in Table I indicate that the unit cell parameters have smaller parameters compared to the literature data. Lower lattice parameters are size-related changes of lattice parameters and present a deficit of the intercrystalline pressure in a small particle. The calculated crystallite size of about 200 nm confirms that as the particle size decreases, the lattice parameter of the nanoparticle decreases.[24] Results of OCP confirm that crystal sizes determine the size-related change of the length of each lattice edge in a perpendicular direction or the above mentioned preferred orientation, as explained in Fig. 1a.[25] Also obtained structural strain of 0.000176 ‰, which indicates the existence of low structural deformations, may be related to the dislocations between small

crystallites. The results of the refined parameters indicate that nanocrystalline octacalcium phosphate with good structural order was obtained by this method.

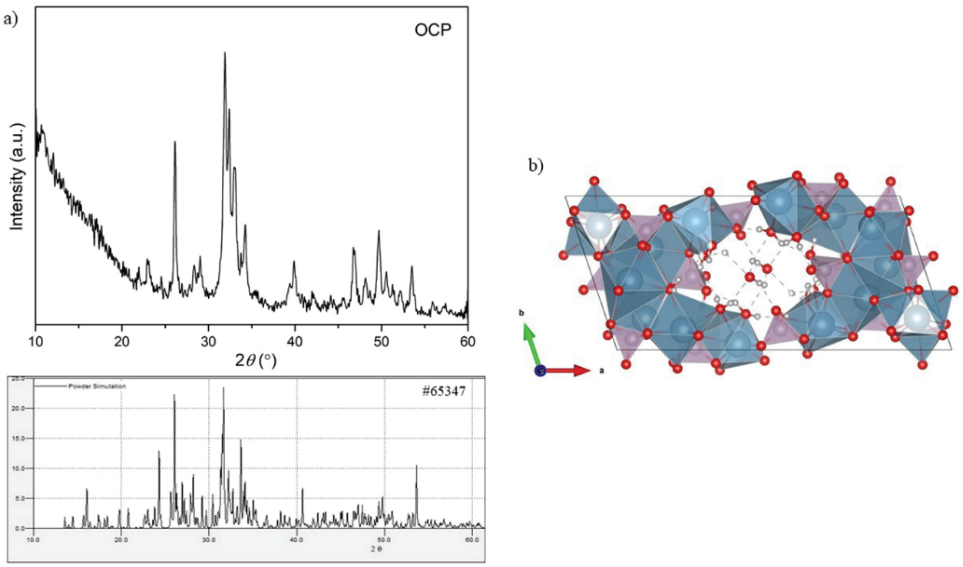

Fig. 2. a) XRD results of OCP with matching card #65347 and b) crystal structure of OCP in the direction of the *c* axis (red spheres are oxygen atoms, grey spheres are hydrogen atoms, hydrogen bonds are shown in dashed lines, PO_4 tetrahedral are presented in purple and CaO_8 octahedral are presented in blue color).

TABLE I. Refinement results; unit cell parameters of synthesized OCP sample

Sample	*a* / Å	*b* / Å	*c* / Å	*α* / °	*β* / °	*γ* / °
ICSD #65347	19.7920(3)	9.6230(3)	6.9350(3)	91.150(3)	93.540(3)	109.650(3)
OCP	19.666(5)	9.519(2)	6.8260(3)	90.120(6)	92.498(4)	108.660(1)

The FTIR-ATR spectra of OCP samples and OCP samples after Pb(II) and Cd(II) removal (OCP_{PC}) are shown in Fig. 3a and b. For both samples, the most dominant peaks are near 1018 and 558 cm^{-1}, which originate from stretching vibrations of P–O bands and bending vibrations of O–P–O, respectively, and can be assigned to the PO_4^{3-} group.[26–29] Additionally, stretching vibration at 865 cm^{-1} can be attributed to the HPO_4^{2-} in the hydrated layers of OCP crystals.[27,29] Crystalline water in samples is represented by a broad peak at 3500 cm^{-1}.[26] Two shoulder straps which can be observed only for pristine OCP sample at 1071 and 1190 cm^{-1} could originate from stretching and bending vibration attributed to the HPO_4^{2-} group in OCP crystal structure (Fig. 3b) and these vibration peaks of PO_4^{3-} and HPO_4^{2-} groups are typical for OCP crystal formation.[27]

From the OCP_{PC} spectrum it can be seen that the main differences, compared to pristine OCP, are the absence of peaks attributed to the HPO_4^{2-} group at

1071 and 1190 cm^{-1} as well as an increase of O–P–O bending vibrations intensity at 600 and 558 cm^{-1} and intensity of stretching vibration at 865 cm^{-1} of HPO_4^{2-} group in the hydrated layers (Fig. 3b).[27,29] These are structural changes of OCP after the adsorption processes of lead and cadmium and the presence of more hydrated layers.

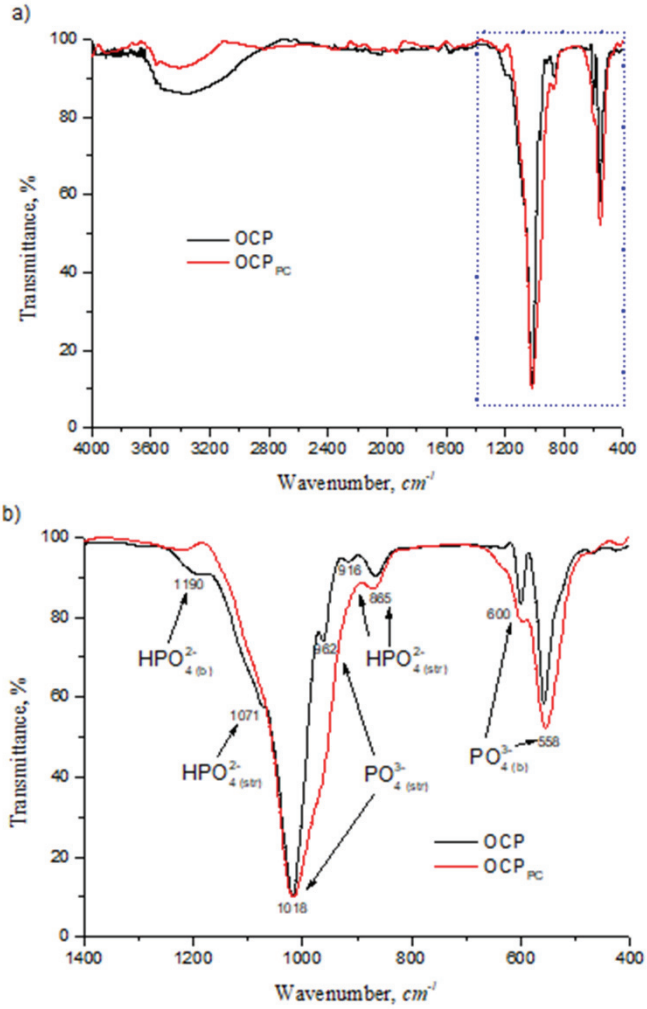

Fig. 3. a) FTIR spectra of OCP and OCP_{PC}; b) amplified image of the square marked area in a.

The summarized results of the adsorption kinetic study and the fitting plots are presented in Table II and Fig. 4, respectively. For Pb(II), in the first 10 min, a very fast removal rate with a rapid increase in adsorption capacity was observed. The equilibrium state was reached after 10 min when it adsorbed more than 98 %

Pb(II). In the case of Cd(II), a fast removal rate, also after 10 min, was observed with a lower adsorption capacity of about 63 %. After 10 min, adsorption was slower, and the equilibrium was reached after 2h of adsorption.

TABLE II. The fitting parameters of adsorption kinetics using the pseudo-first-order

Pollutant	Pseudo-first-order parameters		
	R^2	k_1 / min^{-1}	Q_e calcd. / mg g^{-1}
Cd (II)	0.8755	0.0763	74.84
Pb (II)	0.8359	0.2480	125.87

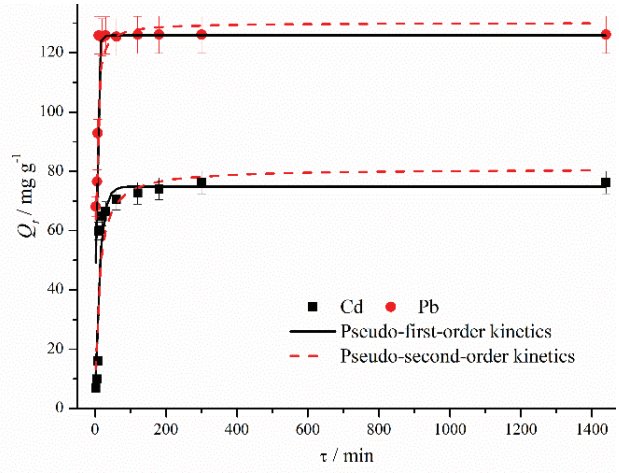

Fig. 4. Adsorption kinetic data for Cd(II) and Pb(II) and nonlinear fit with pseudo-first and pseudo-second-order kinetic models.

Comparing the removal rate after 10 min, it can be concluded that the removal rate of Pb(II) is two times higher than the removal rate of Cd(II) (Fig. 5). The fitting parameters of the adsorption kinetic model are present in Tables II and III. It can be observed that the correlation coefficient (R^2) is very similar for the both theoretical models and the both pollutants (ranged 0.8359–0.8827), but it is slightly higher for pseudo-second-order, and according to this fact, the adsorption of Cd(II) and Pb(II) can be described by the both models which confirm the good agreement, between Q_e experimental and Q_e calculated. According to the recent literature data, the pseudo-second-order model shows better agreement with most adsorption systems in this field. Since there is no adsorbate dissociation in our system, the pseudo-first-order model is the only logical choice to describe the kinetics of Cd(II) and Pb(II) adsorption on the OCP sample.[30] The lower rate constant value for Cd(II) shows that the OCP first adsorb the Cd(II). This observation indicates that the OCP sample has much better adsorption performance for Pb(II) removal in a mixture with Cd(II).

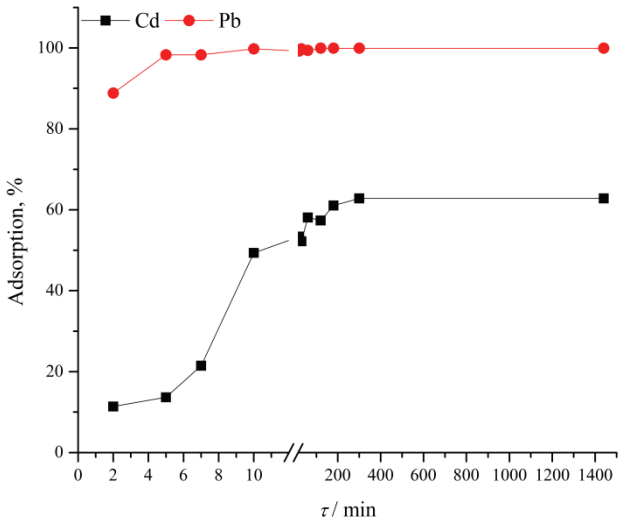

Fig. 5. Adsorption kinetic curves for Cd(II) and Pb(II) adsorption on OCP.

TABLE III. The fitting parameters of adsorption kinetics using the pseudo-second-order models

Pollutant	Pseudo-second-order parameters			Q_e exp. / mg g^{-1}
	R^2	k_2 / g mg min^{-1}	Q_e calcd. / mg g^{-1}	
Cd (II)	0.8827	0.0973	80.90	77.52
Pb (II)	0.8472	0.4805	130.11	128.54

The results of the adsorption isotherms study are presented in Fig. 6 and Tables IV and V. Based on the R^2 value, adsorption data of Cd(II) and Pb(II) could be well described by the Langmuir isotherm model. Theoretical maximum

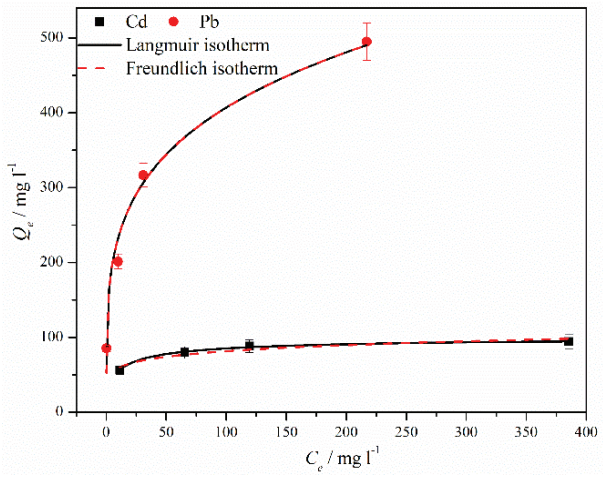

Fig. 6. Adsorption isotherms fitted by Langmuir and Freundlich model.

adsorption capacity (Q_{max}) obtained from Langmuir isotherm is much higher for Pb(II) (1951 mg/g) than Cd(II) (104 mg/g), which confirms excellent adsorption performance of the OCP sample for Pb(II) removal. The shape of the isotherm curve for Pb(II) shows that the plateau stage is not reached, which means that removal of Pb(II) at a higher concentration is possible. Also, the affinity for Pb(II) removal is much higher than the affinity for Cd(II) removal.

TABLE IV. The fitting parameters of Langmuir adsorption isotherm

Pollutant	Parameter		
	R^2	Q_{max} / mg g^{-1}	b / dm^3 mg^{-1}
Cd (II)	0.9863	104	0.2657
Pb (II)	0.9693	1951	6.99×10^{-4}

TABLE V. The fitting parameters of adsorption isotherm using the Freundlich model

Pollutant	Parameter		
	R^2	K_F / mg g^{-1} (dm^3 mg^{-1})$^{1/n}$	$1/n_F$
Cd (II)	0.8920	43.33	0.1373
Pb (II)	0.9248	134.63	0.2403

In order to check the goodness of fit for the Freundlich models in a different range of points, a fitting was done in the middle range of points, with no points at low concentrations and high concentration - near saturation limits. The results are shown in Table VI and Fig. 7. A difference was observed in the case of Pb adsorption. A better agreement of the Freundlich model was established in the middle range of points, which was confirmed by a higher value of the coefficient R^2.

TABLE VI. The fitting parameters of adsorption isotherm for Pb fitted in the middle range of points using the Freundlich model

Pollutant	Parameter		
	R^2	K_F / mg g^{-1} (dm^3 mg^{-1})$^{1/n}$	$1/n_F$
Pb (II)	0.9682	119.50	0.2658

With the aim of better understanding the entire process of removing targeted heavy metal ions from aqueous solutions, XRD analysis of OCP was performed after adsorption experiments. In Fig. 8, the XRD diffractogram of the dried OCP_{PC} sample is presented. On the basis of the presented results, two phases are identified. The peaks primarily belong to the phase declared hexakis(phosphate(V)) dihydroxide – $Pb_{10}(PO_4)_6(OH)_2$, with hexagonal symmetry, *e.g.*, $P6_3/m$. The other identified phase belongs to hydroxyapatite $Ca_5(PO_4)_3OH$ with the same structural property. The identified hydroxyapatite phases are characterized by clear, sharp and well-defined peaks that indicate a good structural arrangement of these phases. A slightly higher background indicates a certain content of

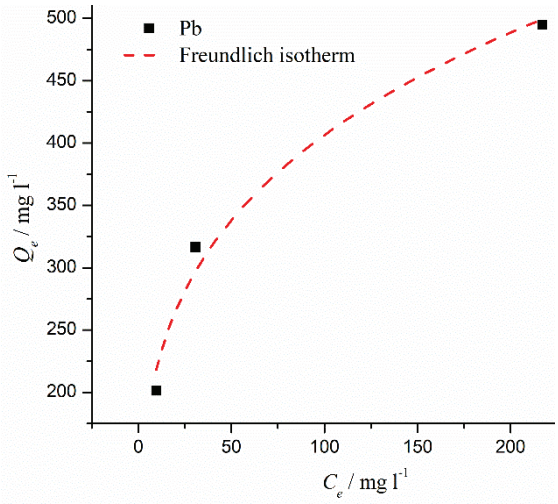

Fig. 7. Adsorption isotherm for Pb fitted in the middle range of points by Freundlich model.

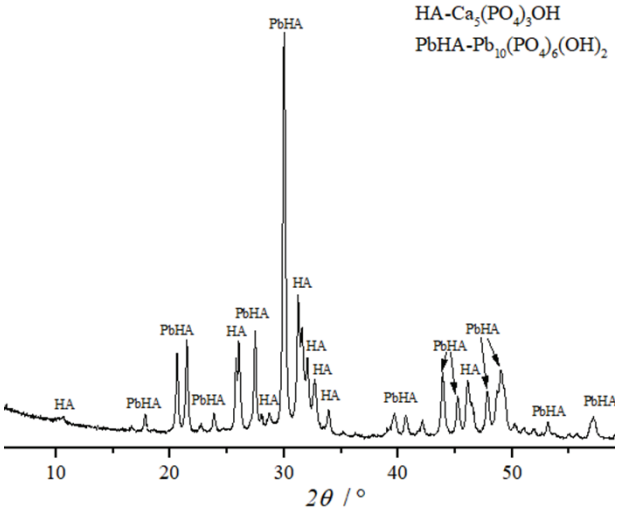

Fig. 8. X-ray powder diffractogram of dried OCP_{PC} sample.

the amorphous phase after adsorption experiments. Based on these analyses, it can be said that phase and structural transformations of octacalcium phosphate occurred in the presence of lead. In the positions where calcium was found, the incorporation of lead and the formation of a hexagonal structure occurred first, along with the formation of hydroxyapatite, which represents a more stable structural hexagonal form into which triclinic octacalcium phosphate tends to convert most often by the dehydration process. This was also confirmed by FTIR-ATR analysis (Fig. 3b). In the OCP structure, the HPO_4–OH layer is unstable in tri-

clinic structure; because of this, it is easily transformed to hydroxyapatite (HAp) *via* dehydration upon further immersion.[31] The same process happened with Pb(II) ions, which made a stable further insoluble salt.

CONCLUSION

The targeted octacalcium phosphate material was successfully obtained by solution precipitation method using acetate and sodium phosphate solutions. The parameters calculated using XRD data show that monocrystalline material was obtained with some lower unit cell parameters compared to data from the literature. FTIR spectra revealed characteristic vibration peaks of PO_4^{3-} and HPO_4^{2-} groups, which are typical for OCP crystal formation. The prismatic and petal-like microstructure of OCP crystal grains is confirmed by SEM analysis, with a 1.33 Ca/P ratio. For Cd(II), the theoretical maximum adsorption capacity was 104 mg/g, and with lower adsorption capacity by about 63 %, while after 10 min adsorption was much slower, and equilibrium was reached after 2h. Excellent adsorption performance of the OCP for Pb(II) removal, which is obtained from Langmuir isotherm, was 1951 mg/g of theoretical maximum adsorption capacity, with up to 98 % of adsorption capacity in the first 10 min. After adsorption experiments, XRD analysis showed the structural transformation of octacalcium phosphate into a hexagonal symmetry structure corresponding to the hydroxyapatite phase. This mechanism of interlocking of lead in the structure of OCP and its translation into a stable, further insoluble lead salt, on the basis of which the use of this material can be recommended for the remediation of soils polluted with high concentrations of lead.

Acknowledgment. The research was funded by the Ministry of Science, Technological Development and Innovation of the Republic of Serbia, in a frame of research topics number 1702302 and 1702307 based on contract number: 451-03-1/2023-03/17.

И З В О Д

УКЛАЊАЊЕ ОЛОВА И КАДМИЈУМА ИЗ ВОДЕНОГ РАСТВОРА КОРИСТЕЋИ ОКТАКАЛЦИЈУМ-ФОСФАТ КАО АДСОРБЕНТ

МИЉАНА М. МИРКОВИЋ[1], ИВАН Д. БРАЦАНОВИЋ[1], АЛЕКСАНДАР Д. КРСТИЋ[2], ДУЊА Д. ЂУКИЋ[3], ВЛАДИМИР М. ДОДЕВСКИ[1] и АНА М. КАЛИЈАДИС[1]

[1]Одсек за материјале, Институт за нуклеарне науке Винча – Национални институт Републике Србије, Универзитет у Београду, Мике Петровића Аласа 12–14, 11000 Београд, [2]Одсек за физичку хемију, Институт за нуклеарне науке Винча – Национални институт Републике Србије, Универзитет у Београду, Мике Петровића Аласа 12–14, 11000 Београд и [3]Универзитет у Београду, Биолошки факултет, Студентски трг 16, 11000 Београд

Октакалцијум-фосфат (OCP) је материјал из групе калцијум-фосфата са кристалном структуром сличном хидроксиапатитској. Испитиван је процес уклањања олова и кадмијума у воденом раствору коришћењем синтетисаног октакалцијум-фосфата. Октакалцијум-фосфатни материјал је синтетисан методом преципитације из раствора. Структурна и фазна својства OCP одређена су методом рендгенске дифракције на поли-

кристалном узорку пре и након процеса уклањања полутаната из раствора. Методе скенирајуће електронске микроскопије са енергетско дисперзивном рендгенском спектроскопијом коришћене су за одређивање микроструктурне и семи-квантитативне анализе синтетисаног материјала (SEM-EDS). Карактеристичне траке и одређивање функционалних група одређиване су коришћењем инфрацрвене спектроскопије са Фоуриеровом трансформацијом са ослабљеном тоталном рефлексијом (FTIR-ATR). За циљне загађиваче изабрани су кадмијум и олово у експериментима адсорпције. Резултати показују да OCP у првих 10 min има изузетну брзину уклањања олова; равнотежно стање је постигнуто након 10 min са више од 98 % ефикасности адсорпције. За кадмијум резултати показују исту брзину уклањања али нешто нижу ефикасност адсорпције која износи око 63 %.

(Примљено 15. септембра, ревидирано 4. октобра,- прихваћено 26. децембра 2023)

REFERENCES

1. T. Yokoi, M. Kamitakahara, C. Ohtsuki, *Dalton Trans.* **44** (2015) 7943 (https://doi.org/10.1039/C4DT03943B)
2. R. Hamai, S. Sakai, Y. Shiwaku, T. Anada, K. Tsuchiya, T. Ishimoto, T. Nakano, O. Suzuki, *Appl. Mater. Today* **26** (2022) 101279 (https://doi.org/10.1016/j.apmt.2021.101279)
3. O. Suzuki, R. Hamai, S. Sakai, *Acta Biomater.* **158** (2023) 1 (https://doi.org/10.1016/j.actbio.2022.12.046)
4. S.V. Dorozhkin, M. Epple, *Angew. Chem. Int. Ed.* **41** (2002), 3130 (https://doi.org/10.1002/1521-3773(20020902)41:17<3130::AID-ANIE3130>3.0.CO;2-1)
5. A. Idini, E. Dore, D. Fancello, F. Frau, *Heliyon* **5** (2019) e02288 (https://doi.org/10.1016/j.heliyon.2019.e02288)
6. I. Yamada, M. Tagaya, *Colloid Interface Sci. Commun.* **30** (2019) 100182 (https://doi.org/10.1016/j.colcom.2019.100182)
7. Z. Jianhu, S. Jiacai, Y. Xiaojun, S. Yiping, *J. Mater.* **55** (2020) 7502 (https://doi.org/10.1007/s10853-020-04539-0)
8. W.E. Brown, M. Mathew, M.S. Tung, *Prog. Cryst. Growth Charact.* **4** (1981) 59 (https://doi.org/10.1016/0146-3535(81)90048-4)
9. T. Yokoi, S. Machida, Y. Sugahara, M. Hashimoto, S. Kitaoka, *Chem. Commun.* **53** (2017), 6524 (https://doi.org/10.1039/C7CC01169E)
10. R. O'Sullivan, D. Kelly, in *Octacalcium Phosphate Biomaterials*, O. Suzuki, G. Insley, Eds., Woodhead Publishing, Sawston, 2020, pp. 147–176 (https://doi.org/10.1016/B978-0-08-102511-6.00007-8)
11. M.J. Arellano-Jiménez, R. García-García, J. Reyes-Gasga, *J. Phys. Chem. Solids* **70** (2009) 390 (https://doi.org/10.1016/j.jpcs.2008.11.001)
12. S. Mandel, A.C. Tas, *Mater. Sci. Eng., C* **30** (2010) 245 (https://doi.org/10.1016/j.msec.2009.10.009)
13. O. Suzuki, *Acta Biomater.* **6** (2010) 3379 (https://doi.org/10.1016/j.msec.2009.10.009)
14. P. Sharma, S. Sangwan, S. Mehta, in *Engineered Nanomaterials for Sustainable Agricultural Production, Soil Improvement and Stress Management*, A. Husen, Ed., Academic Press, Cambridge, MA, 2023, pp. 71–97 (https://doi.org/10.1016/B978-0-323-91933-3.00008-8)
15. A.L. Patterson, *Phys. Rev.* **56** (1939) 978 (https://doi.org/10.1103/PhysRev.56.978)

16. W.K. Nolze, *J. Appl. Cryst.* **29** (1996) 301 (https://doi.org/10.1107/S0021889895014920)
17. A. Krstić, A. Lolić, M. Mirković, J. Kovač, T. M. Arsić, B. Babić, A. Kalijadis, *J. Environ. Chem. Eng.* **10** (2022) 108998 (https://doi.org/10.1016/j.jece.2022.108998)
18. J. Zhu, J. Shu, X. Yue, Y. Su, *J. Mater. Sci.* **55** (2020) 7502 (https://doi.org/10.1007/s10853-020-04539-0)
19. T. Miyazaki, Y. *Mater. Lett.X* **15** (2022) 100151 (https://doi.org/10.1016/j.mlblux.2022.100151)
20. X. Zhao, S. Jiang, J. Rao, J. Zhou, Z. Li, J. Yang, K. Yan, H. Shi, *Mater. Lett.* **328** (2022) 133137 (https://doi.org/10.1016/j.matlet.2022.133137)
21. M. Asadi-Eydivand, M. Solati-Hashjin, A. Farzadi, N.A.A. Osman, *Ceram. Int.* **40** (2014) 12439 (https://doi.org/10.1016/j.ceramint.2014.04.095)
22. K. Onuma, M.M. Saito, Y. Yamakoshi, M. Iijima, Y. Sogo, K. Momma, *Acta Biomater.* **125** (2021) 333 (https://doi.org/10.1016/j.actbio.2021.02.024)
23. H.B. Lu, C.L. Ma, H. Cui, L.F. Zhou, R.Z. Wang, F.Z. Cui, *J. Cryst. Growth* **155** (1995) 120 (https://doi.org/10.1016/0022-0248(95)00229-4)
24. W.H. Qi, M.P. Wang, Y.C. Su, *J. Mater. Sci. Lett.* **21** (2002) 877 (https://doi.org/10.1023/A:1015778729898)
25. M. Ya Gamarnik, *Phys. Status Solidi, B* **178** (1993) 59 (https://doi.org/10.1002/pssb.2221780105)
26. X. Zhao, S. Jiang, J. Rao, J. Zhou, Z. Li, J. Yang, K. Yan, H. Shi, *Mater. Lett.* **328** (2022) 133137 (https://doi.org/10.1016/j.matlet.2022.133137)
27. J. Liu, F.Qiu, Y. Zou, Z. Zhang, A. Wang, Y. Zhang, *Ceram. Int.* **49** (2023) 20315 (https://doi.org/10.1016/j.ceramint.2023.03.155)
28. A. Ressler, T. Ivanković, I. Ivanišević, M. Cvetnić, M. Antunović, I. Urlić, H. Ivanković, M. Ivanković, *Ceram. Int.* **49** (2023) 11005 (https://doi.org/10.1016/j.ceramint.2022.11.295)
29. H. Shi, X. Ye, J. Zhang, T. Wu, T. Yu, C. Zhou, J. Ye, *Bioact. Mater.* **6** (2021), 1267 (https://doi.org/10.1016/j.bioactmat.2020.10.025)
30. Y.S. Ho, G. McKay, *Process Biochem.* **34** (1999) 451 (https://doi.org/10.1016/S0032-9592(98)00112-5)
31. Y. Sugiura, Y. Makita, *J. Cryst. Growth* **583** (2022) 126545 (https://doi.org/10.1016/j.jcrysgro.2022.126545).